Two-Dimensional Metals for Piezoelectriclike Devices Based on Berry-Curvature Dipole

Rui-Chun Xiao,[1,2] Ding-Fu Shao,[3] Zhi-Qiang Zhang,[1] and Hua Jiang[1,2,*]

[1] *School of Physical Science and Technology, Soochow University, Suzhou 215006, China*

[2] *Institute for Advanced Study, Soochow University, Suzhou 215006, China*

[3] *Department of Physics and Astronomy Nebraska Center for Materials and Nanoscience, University of Nebraska, Lincoln, Nebraska 68588-0299, USA*

(Received 10 October 2019; revised manuscript received 21 January 2020; accepted 18 March 2020; published 7 April 2020)

Piezotronics is an emerging field, which exploits strain to control the transport properties in condensed matters. At present, piezotronics research majorly focuses on insulators with tunable electric dipole by strain. Metals are excluded in this type of application due to the absence of the electric dipole. The recently discovered Berry-curvature dipole can exist in metals, consequently introduces the possibility of the piezoelectric phenomena in them. In this paper, we predict that strain can switch the Berry-curvature dipole, and lead to the nonlinear Hall effect in the two-dimensional (2D) $1H$-MX_2 (M = Nb, Ta; X = S, Se). Based on symmetry analysis and first-principles calculations, we show these 2D monolayer metals have the desired piezoelectriclike property: without strain, the Berry-curvature dipole is eliminated by symmetry, prohibiting the nonlinear Hall effect; while uniaxial strain can effectively reduce the symmetry to introduce sizable Berry-curvature dipole, and it can generate observable Hall voltage under a reasonable experimental condition. Due to the nonlinear and topological properties, the piezoelectriclike property here is quite different from the traditional one based on the electric dipole. Compared with the traditional piezoelectric materials, which can only exist in insulators, we manifest that the 2D metallic $1H$-MX_2 (M = Nb, Ta; X = S, Se) can be applied in the platform for piezoelectriclike devices such as strain sensors, terahertz detections, energy harvesters etc.

DOI: 10.1103/PhysRevApplied.13.044014

I. INTRODUCTION

The general piezoelectric effect is understood as the linear electromechanical interaction between the mechanical and the electrical state in crystalline materials without inversion symmetry. However, in most application scenarios, piezotronics deals with the fabrication of the device using the piezopotential as a "gate" voltage to tune and control charge-carrier transport across metal-semiconductor contacts or p-n junctions [1], i.e., piezoelectric devices transfer force signals into electric ones. Piezotronics as a research field has attracted growing interests for electronic applications in sensors, transducers, power generation, etc. [2–11]. Piezotronics exploits the piezoelectric potential created in materials to control the transport properties. Special interest has been focused on two-dimensional (2D) piezoelectric materials [12–14], due to the convenience of strain application and ability to withstand the enormous strain. Electric dipole **P** can be orderly arranged by strain in solids, due to the transitions between nonpolar and polar symmetries. Such a mechanism becomes the focus of piezoelectricity research [12–18]. The current piezotronics researches majorly focus on the insulators, because **P** in metals will be neutralized by free electrons. Exploration of an analogy of **P** will be helpful to lead piezoresponse in metal for the piezoelectriclike applications.

The Berry-curvature dipole **D** [19,20] was proposed recently and might provide an avenue to introduce desired piezoelectriclike properties in metals. **D** is the measure of the separation of positive and negative Berry-curvature in reciprocal space. **D** relates to the electronic states at the Fermi surface, so it can only exist in metals. **D** can generate second-order anomalous transport phenomena in the absence of magnetic field, i.e., nonlinear Hall effect [19], which was confirmed in bilayer 2D WTe_2 by experiments [21–23] recently. Similar with **P** [18,20], the emergence of **D** also requires the crystal symmetry [19]. Except for bilayer 2D WTe_2, the symmetries of most 2D materials force the **D** to be zero [24,25]. Since strain can be easily applied in 2D materials to change the symmetry and switch **D**, a 2D metal piezoelectriclike device based on nonlinear Hall effect can be fabricated, as shown in Fig. 1. In such

*jianghuaphy@suda.edu.cn

 © 2020 American Physical Society

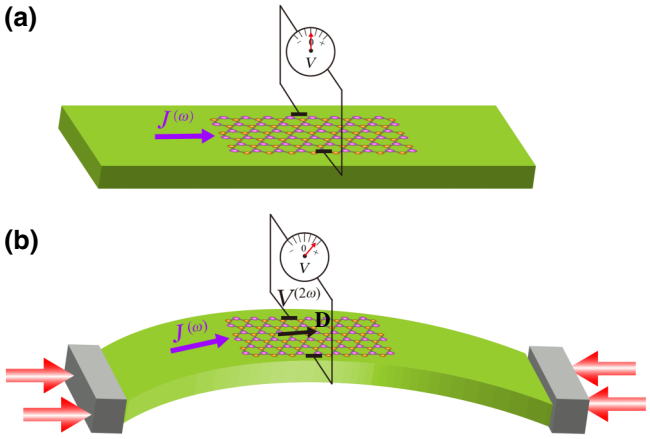

FIG. 1. Metallic piezoelectriclike device based on Berry-curvature dipole **D**. Charge current $J^{(\omega)}$ leads to (a) zero nonlinear Hall voltage without strain due to the vanishing of **D**, and (b) finite nonlinear Hall voltage $V^{(2\omega)}$ with uniaxial strain due to the emerging of **D**.

a device, **D** is zero for the pristine 2D metal, leading to zero nonlinear Hall voltage [Fig. 1(a)]. Strain can break the crystal symmetry, lead to finite **D**, and may generate observable nonlinear Hall voltage [Fig. 1(b)]. Transition-metal dichalcogenides (TMDs) of 1H-phase monolayers are one of the most investigated 2D material categories, and are candidates to realize such a piezoelectriclike device. Uniaxial strain can be used to reduce the symmetry of 1H-MX_2 and switch **D**. It has been discussed that the uniaxial strain can introduce the nonlinear Hall effect in 1H-MoS_2 and 1H-WSe_2[19,26,27]. However, these two materials are semiconductors, and the emergence of **D** also requires the complemental electric doping, which limits the piezoelectriclike application based on the nonlinear Hall effect. Intrinsic 2D metallic 1H-MX_2 (M = Nb, Ta; X = S, Se) might be more suitable candidates to realize such piezoelectriclike devices. The strain should be able to switch the **D** in 2D metals, as strain manipulates **P** in semiconductor 1H-MoS_2 [12–14,18].

In this work, using symmetry analysis and first-principles calculations, we show that monolayer metallic 1H-MX_2 (M = Nb, Ta; X = S, Se) can be applied in the piezoelectriclike devices based on Berry-curvature dipole. Without strain, **D** in these materials is zero due to the symmetry restriction, prohibiting the nonlinear Hall effect. Small uniaxial strain (along zigzag or armchair direction) can effectively reduce the symmetry and generate sizable **D**, leading to observable nonlinear Hall voltage in a conventional experimental condition. Since the traditional piezoelectricity induced by electric dipole **P** has wide applications in both electronic and piezotronic devices [18], the piezoelectriclike property based on the Berry-curvature dipole **D** should also have a significant impact on the development of piezotronics devices.

The rest of the paper is organized as follows. In Sec. II, we introduce how to use the strain to break the symmetry and switch **D** in 1H-MX_2 (M = Nb, Ta; X = S, Se). In Sec. III, we introduce the first-principles calculation methods. The calculation results and corresponding explanations are shown in Sec. IV. Discussion of the characteristics of piezoelectriclike devices is listed in Sec. V. A brief conclusion is in Sec. VI.

II. SYMMETRY ANALYSIS

In order to get the piezoelectriclike effect, the nonlinear Hall effect should be very small or zero without strain, while greatly enhanced under strain. Since nonlinear Hall signal is proportional to Berry-curvature dipole **D**, and **D** is highly related to the symmetry. We analyze the symmetries of **D** with and without strain for 1H-MX_2 (M = Nb, Ta; X = S, Se) first.

Since 1H-MX_2 (M = Nb, Ta; X = S, Se) has time-reversal symmetry $\mathcal{T}$, but no inversion symmetry $\mathcal{I}$, we start with analyzing the Berry-curvature dipole **D** under these two types of symmetry. As preliminary, we analysis the symmetry of Berry-curvature $\Omega_{n,a}(\mathbf{k})$ first. $\Omega_{n,a}(\mathbf{k})$ is odd under the time-reversal symmetry, i.e., $\mathcal{T}$: $\Omega_{n,a}(\mathbf{k}) = -\Omega_{n,a}(-\mathbf{k})$, where n is the band index and $a \in \{x, y, z\}$. Therefore, the integration of $\Omega_{n,a}(\mathbf{k})$ of occupied states in a nonmagnetic (time-reversal invariant) material is zero, and it is the reason why the anomalous Hall effect cannot appear in nonmagnetic materials. Besides, $\Omega_{n,a}(\mathbf{k})$ is even with respect to inversion symmetry, $\mathcal{I}$: $\Omega_{n,a}(\mathbf{k}) = \Omega_{n,a}(-\mathbf{k})$. Hence, under time-reversal symmetry $\mathcal{T}$ and inversion symmetry $\mathcal{I}$, the $\Omega_{n,a}(\mathbf{k})$ is zero at every **k** point. Therefore, it is necessary to break the inversion symmetry $\mathcal{I}$ to obtain the local Berry-curvature in nonmagnetic systems.

Berry-curvature dipole **D** is a 3 × 3 tensor, and D_{bd} is an element of **D**, defined as

$$D_{bd} = -\sum_n \int \frac{\partial f_n(\mathbf{k})}{\partial \epsilon_n(\mathbf{k})} v_b \Omega_{n,d}(\mathbf{k}) d[\mathbf{k}] = \int d_{bd} d[\mathbf{k}], \quad (1)$$

where $d_{bd}(\mathbf{k})$ is the Berry-curvature-dipole density

$$d_{bd}(\mathbf{k}) = -\sum_n \frac{\partial f_n(\mathbf{k})}{\partial \epsilon_n(\mathbf{k})} v_b \Omega_{n,d}(\mathbf{k}), \quad (2)$$

$f_n(\mathbf{k})$ refers to the Fermi distribution, and $v_b = \partial \epsilon_n(\mathbf{k})/\partial \mathbf{k}_b$ is the electron velocity. The factor $\partial f_n(\mathbf{k})/\partial \epsilon_n(\mathbf{k})$ in Eq. (1) implies D_{bd} is a Fermi surface determined quantity. $d_{bd}(\mathbf{k})$ is even with respect to the time-reversal symmetry and odd under the inversion symmetry according to Eq. (2), which

is opposite to the case of the Berry curvature, i.e.,

$$\begin{cases} \mathcal{T} : d_{bd}(\mathbf{k}) = d_{bd}(-\mathbf{k}), \\ \mathcal{I} : d_{bd}(\mathbf{k}) = -d_{bd}(-\mathbf{k}). \end{cases} \tag{3}$$

Therefore, when $\mathcal{I}$ is broken, nonzero D_{bd} can emerge in a nonmagnetic metal, i.e., the nonlinear Hall current might appear.

Different from **P**, **D** is a pseudotensor and determined by [19]

$$\mathbf{D} = \det(S) S \mathbf{D} S^{-1}, \tag{4}$$

where S denotes the symmetric operation matrix of the point group. Specifically, since Berry curvature $\Omega_{n,a}(\mathbf{k})$ only has a z component in a 2D system, only D_{xz} and D_{yz} exist in 2D materials. In other words, **D** transforms as a pseudovector in the 2D systems. In $1H$ monolayers transition-metal dichalcogenides, the point group D_{3h} ($\bar{6}m2$) contains a threefold rotation $\mathcal{C}_3$ symmetry along z direction ($\mathcal{C}_{3z}$), one mirror reflection perpendicular to z direction ($\mathcal{M}_{xy}$), three mirrors are parallel to z direction and three in-plane $\mathcal{C}_2$ symmetries [Fig. 2(a)]. The $\mathcal{C}_{3z}$, $\mathcal{C}_{2y}$, and $\mathcal{M}_{xy}$ are the generator operators of D_{3h}:

$$\mathcal{C}_{3z} = \begin{pmatrix} \cos(2\pi/3) & -\sin(2\pi/3) & 0 \\ \sin(2\pi/3) & \cos(2\pi/3) & 0 \\ 0 & 0 & 1 \end{pmatrix}, \tag{5}$$

$$\mathcal{C}_{2y} = \begin{pmatrix} -1 & 0 & 0 \\ 0 & 1 & 0 \\ 0 & 0 & -1 \end{pmatrix}, \tag{6}$$

$$\mathcal{M}_{xy} = \begin{pmatrix} 1 & 0 & 0 \\ 0 & 1 & 0 \\ 0 & 0 & -1 \end{pmatrix}. \tag{7}$$

Under these symmetry operators, **D** transforms as according to Eq. (4):

$$\det(\mathcal{C}_{3z})\mathcal{C}_{3z}\mathbf{D}\mathcal{C}_{3z}^{-1} = \begin{pmatrix} \frac{1}{4}\left(D_{xx}+3D_{yy}\right)+\frac{\sqrt{3}}{4}\left(D_{yx}+D_{xy}\right) & \frac{\sqrt{3}}{4}\left(-D_{xx}+D_{yy}\right)+\frac{1}{4}\left(D_{xy}-3D_{yx}\right) & -\frac{D_{xz}}{2}-\frac{\sqrt{3}D_{yz}}{2} \\ \frac{\sqrt{3}}{4}\left(-D_{xx}+D_{yy}\right)+\frac{1}{4}\left(-3D_{xy}+D_{yx}\right) & \frac{1}{4}\left(3D_{xx}+D_{yy}\right)-\frac{\sqrt{3}}{4}\left(D_{yx}+D_{xy}\right) & \frac{\sqrt{3}D_{xz}}{2}-\frac{D_{yz}}{2} \\ -\frac{D_{zx}}{2}-\frac{\sqrt{3}D_{zy}}{2} & \frac{\sqrt{3}D_{zx}}{2}-\frac{D_{zy}}{2} & D_{zz} \end{pmatrix}, \tag{8}$$

$$\det(\mathcal{C}_{2y})\mathcal{C}_{2y}\mathbf{D}\mathcal{C}_{2y}^{-1} = \begin{pmatrix} D_{xx} & -D_{xy} & D_{xz} \\ -D_{yx} & D_{yy} & -D_{yz} \\ D_{zx} & -D_{zy} & D_{zz} \end{pmatrix}, \tag{9}$$

$$\det(\mathcal{M}_{xy})\mathcal{M}_{xy}\mathbf{D}\mathcal{M}_{xy}^{-1} = \begin{pmatrix} -D_{xx} & -D_{xy} & D_{xz} \\ -D_{yx} & -D_{yy} & D_{yz} \\ D_{zx} & D_{zy} & -D_{zz} \end{pmatrix}. \tag{10}$$

The $\mathcal{C}_{3z}$ symmetry ensures the vanishing of D_{xz} and D_{yz} according to Eqs. (4) and (8). Besides, the other **D** elements are all zeros under D_{3h} symmetry by combination of Eqs. (4) and (8)–(10). In other words, there is no **D** in $1H$-MX_2 (M = Nb, Ta; X = S, Se) without strain.

When armchair or zigzag strain is applied, the $\mathcal{C}_{3z}$ rotation symmetry is broken; however, the $\mathcal{M}_{xy}$, $\mathcal{C}_{2y}$, and $\mathcal{M}_{yz}$ are preserved [Fig. 2(a)], leading to a C_{2v} point-group symmetry. That is to say, Eqs. (9) and (10) still satisfy Eq. (4), while Eq. (8) does not. We can get the symmetry of **D** under C_{2v}:

$$\mathbf{D} = \begin{pmatrix} 0 & 0 & D_{xz} \\ 0 & 0 & 0 \\ D_{zx} & 0 & 0 \end{pmatrix}. \tag{11}$$

$\mathcal{C}_{2y}$ and $\mathcal{M}_{yz}$ guarantee the vanishing of D_{yz}, however D_{xz} is nonzero under C_{2v} symmetry. Therefore, the switching of the finite and zero **D** can be realized in a metallic $1H$-MX_2 by applying and releasing uniaxial strain. With the appearance of the finite Berry-curvature dipole, the nonlinear Hall effect can exist in these 2D nonmagnetic metals. These materials may be used as piezoelectriclike devices.

The method to fabricate the piezoelectriclike devices utilizing **D** is different from the conventional one based on **P** [12–18]. For example, from above symmetry constrain **D** (D_{xz}) is perpendicular to the polar axis ($\mathcal{C}_{2y}$), opposite to **P**, which is along the polar axis. The difference between **D** and **P** is results from that **P** is a polar vector, while **D** is an axial tensor (or axial vector in 2D). In contrast to Eq. (4),

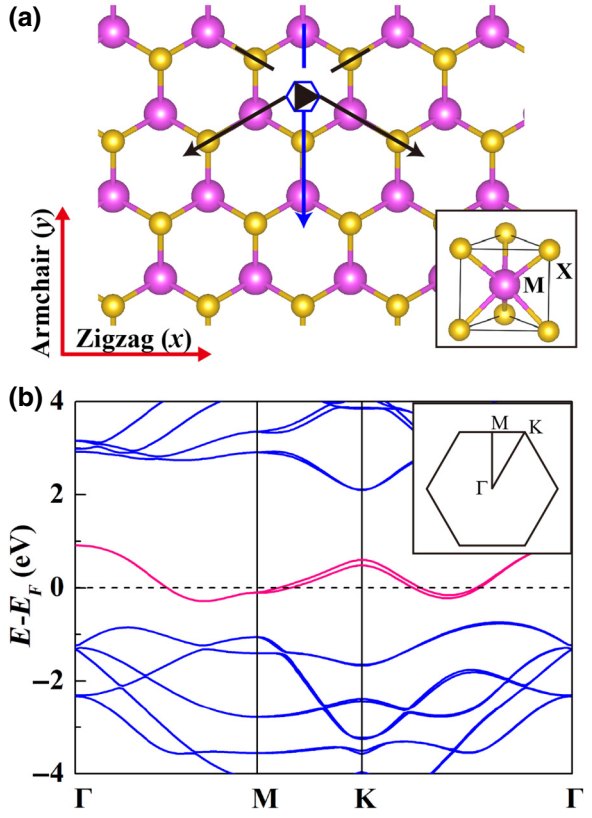

FIG. 2. (a) Crystal structure of monolayer $1H$-MX_2 (M = Nb, Ta; X = S, Se). The arrows represent the in-plane $\mathcal{C}_2$ symmetries, line segments represent vertical mirror symmetries and hollowed hexagon denotes for the $\mathcal{C}_{3z}$ and $\mathcal{M}_{xy}$ symmetries. The symmetries in black (blue) are broken (unbroken) when uniaxial strain is applied. (b) Band structure of monolayer $1H$-NbS_2. The inset illustrates the Brillouin zone.

P is determined by

$$\mathbf{P} = S\mathbf{P}. \tag{12}$$

The differences between Berry-curvature dipole and electric dipole are summarized in Table I.

The **D** and **P** can coexist in specific symmetry, which connects to the ferroelectricity [28,29].

III. CALCULATION DETAILS

From the above descriptions, the strain can switch **D** from zero to finite value in $1H$-MX_2 (M = Nb, Ta; X = S, Se). Thus these materials can in principle be used as piezoelectric devices. Nevertheless, the value of **D** and whether it can induce an observable nonlinear Hall effect need to be calculated.

The first-principles calculations based on density functional theory (DFT) were performed by using the QUANTUM-ESPRESSO package [30]. Ultrasoft pseudopotentials and general gradient approximation (GGA) according to the Perdew-Burke-Ernzerhof (PBE) functional are used.

TABLE I. Comparison between electric dipole **P** and Berry-curvature dipole **D**.

	P	**D**
Tensor type	Polar vector	Axial tensor
Existing space	Real space	Reciprocal space
Existing material	Insulators	Metals
Direction	Parallel to polar axis	Perpendicular to polar axis
Symmetery constraint	Eq. (12)	Eq. (4)
Resulting phenomenon	Surface charge accumulation (piezoelectricity)	Nonlinear Hall effect (piezoelectriclike property)

The energy cutoff of the plane wave (charge density) basis is set to 50 Ry (500 Ry). The Brillouin zone is sampled with a $12 \times 12 \times 1$ mesh of **k** points. To simulate the monolayer, a 20 Å vacuum layer is introduced. The DFT Bloch wave functions are projected to maximally localized Wannier functions by the Wannier90 code [31,32]. The Berry curvature Ω and Berry-curvature dipole **D** are calculated by the WannierTools software package [33]. In the Berry-curvature-dipole calculations, the convergence test is taken, and **k** mesh grids of 600×600 are adopted. The lattice parameters and atomic positions are fully relaxed until the force on each atom is less than 10^{-4} eV/Å. For the samples with uniaxial strain, the atomic positions are relaxed with the lattice parameter fixed to strain.

IV. RESULTS AND EXPLANATIONS

Monolayer $1H$-MX_2 (M = Nb, Ta; X = S, Se) were successfully synthesized in experiment recently [34–39]. In these materials, one M atom and the nearest six X atoms compose a trigonal prism as shown in Fig. 2(a), forming a structure with $P\bar{6}m2$ space group (D_{3h} point-group symmetry) without inversion symmetry. There is one less d electron in the M atom compared with $1H$-MoX_2 and WX_2, leading to the metallic ground states. Nonzero Berry-curvature-dipole density $d_{bd}(\mathbf{k})$ can be introduced without additional doping due to the existence of finite Fermi surface, unlike the semiconductors $1H$-MoS_2 and $1H$-WSe_2 [19,26,27]. These four materials show similar band structures, and here we use $1H$-NbS_2 as a representative.

Figure 2(b) shows the band structure of pristine $1H$-NbS_2. Considering spin-orbit coupling, there are two half-filled bands crossing the Fermi level (E_F). The largest spin-orbit gap of 116 meV between these two bands is found at the K point. These bands form the Fermi surfaces as shown in Fig. 3(a), where two hexagonal hole pockets located at the Γ point and two rounded triangular hole pockets at the K point. The split of two hole pockets around the K point is much larger than that around the Γ point. Figure 3(b) exhibits the distribution of Berry curvature Ω_z

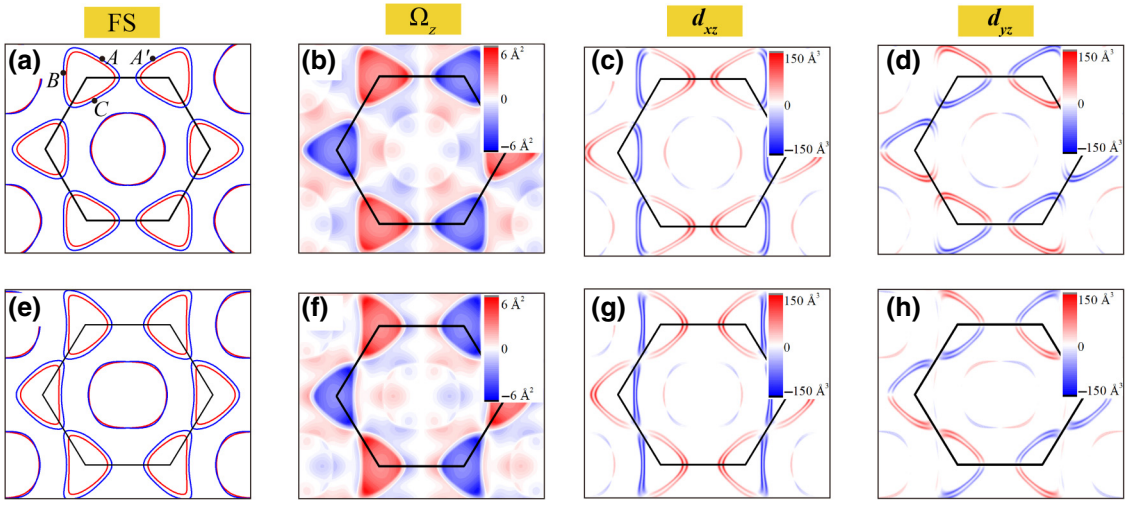

FIG. 3. (a)–(d) Upper panel: (a) Fermi surfaces, (b) Berry curvature $\Omega_z(\mathbf{k})$, (c) Berry-curvature density $d_{xz}(\mathbf{k})$ and (d) $d_{yz}(\mathbf{k})$ of pristine $1H$-NbS_2. Lower panel: (e)–(h) are the same as (a)–(d) with a tensile strain of $\xi = 4\%$ along the armchair direction.

of the occupied bands in the Brillouin zone. As discussed in Sec. II, Ω_z is odd under the time-reversal symmetry, i.e., $\Omega_z(\mathbf{k}) = -\Omega_z(-\mathbf{k})$. The largest Ω_z locates around the K point.

Figures 3(c) and 3(d) plot the Berry-curvature-dipole density d_{xz} and d_{yz}. Since the Berry-curvature dipole is a Fermi-surface-dependent quantity, d_{xz} and d_{yz} are nonzero only on the Fermi lines [see Figs. 3(c) and 3(d)]. We find the largest values of d_{xz} and d_{yz} are around the Fermi pockets surrounding K point as well. d_{xz} and d_{yz} is even under time-reversal symmetry [Eq. (3)], as shown in Figs. 3(c) and 3(d). However, these nonzero d_{xz} and d_{yz} are not sufficient to cause the emergence of **D**, due to the presence of the $\mathcal{C}_{3z}$ symmetry as discussed in Sec. II. It can also be simply explained by comparing Ω_z and velocities v_x and v_y under the $\mathcal{C}_{3z}$ symmetry. The $\mathcal{C}_{3z}$ rotation symmetry can transform the point A in the Fermi surface to points B and C, as shown in Fig. 2(a). $\mathcal{C}_{3z}$ does not change the value of Ω_z of these three points, i.e., $\Omega_z(A) = \Omega_z(B) = \Omega_z(C)$. However, $\mathcal{C}_{3z}$ alters the velocities, leading to $\mathbf{v}(A) + \mathbf{v}(B) + \mathbf{v}(C) = 0$ (see Fig. 6 in Appendix A). Therefore, the integration of the d_{xz} and d_{yz} over the Brillouin zone leads to the vanishing of D_{xz} and D_{yz} according to Eq. (1). The zero **D** of the free-standing materials is important to piezotronics devices because at this case symmetry breaking can switch **D** obviously.

Uniaxial strain (along armchair or zigzag direction) can reduce the symmetry of $1H$-MX_2 to point group C_{2v}. We show the Fermi surfaces, corresponding Berry curvature Ω_z, $d_{xz}(\mathbf{k})$ and $d_{yz}(\mathbf{k})$ under the tensile strain of $\xi = 4\%$ along the armchair direction in Figs. 3(e)–3(h), respectively. We find the shapes of Fermi pockets are significantly changed [Fig. 3(e)]. When the $\mathcal{C}_{3z}$ rotation symmetry is broken, $\mathbf{v}(A) + \mathbf{v}(B) + \mathbf{v}(C) \neq 0$. However, the D_{yz} is still vanishing. This is due to the preserved $\mathcal{C}_{2y}$ symmetry in this point group. $\mathcal{C}_{2y}$ transforms point A to A', and changes the sign of Ω_z, i.e., $\Omega_z(A) = -\Omega_z(A')$. Since $\mathcal{C}_{2y}$ does not influence v_y, and $v_y(A) = v_y(A')$, D_{yz} is enforced to be zero, according to Eq. (1). Fortunately, D_{xz} is nonzero under uniaxial strain. The symmetry of **D** from the first-principles calculations agrees with that from macroscopic perspective as Eq. (11). The nonzero D_{xz} means Berry-curvature dipole **P** along the x direction, i.e., zigzag direction, which is different from the electric dipole **P** of semiconductors $1H$-MX_2 in piezoelectricity experiments [13,16]. The strain-induced Berry-curvature dipole becomes the source of magnetization when there is an in-plane electric field [40], and it can generate the nonlinear Hall effect in nonmagnetic materials.

Figure 4 exhibits D_{xz} of $1H$-NbS_2 under the both armchair and zigzag strain. In the presence of strain, nonzero D_{xz} emerges suddenly and changes linearly with the strain.D_{xz} is relatively large at the Fermi level, and it can be optimized under small electric gate voltage. As shown in Fig. 4, there are two significant features: (1) D_{xz} changes its symbol under tensile and compressive strain, and are basically opposite; (2) D_{xz} under zigzag tensile (compressive) strain shows similar effects with D_{xz} under the armchair compressive (tensile) strain due to the equivalent impact on the crystal and band structures. Two such features show the dependence of D_{xz} under strain and can be used to manipulate the Berry-curvature dipole in the real experiments. We also calculate the Berry-curvature dipole under armchair strain for $1H$-$NbSe_2$, $1H$-TaS_2, and $1H$-$TaSe_2$ as plotted in Fig. 7. We find the strain effect on D_{xz} of these three materials shows similar behavior with that of $1H$-NbS_2.

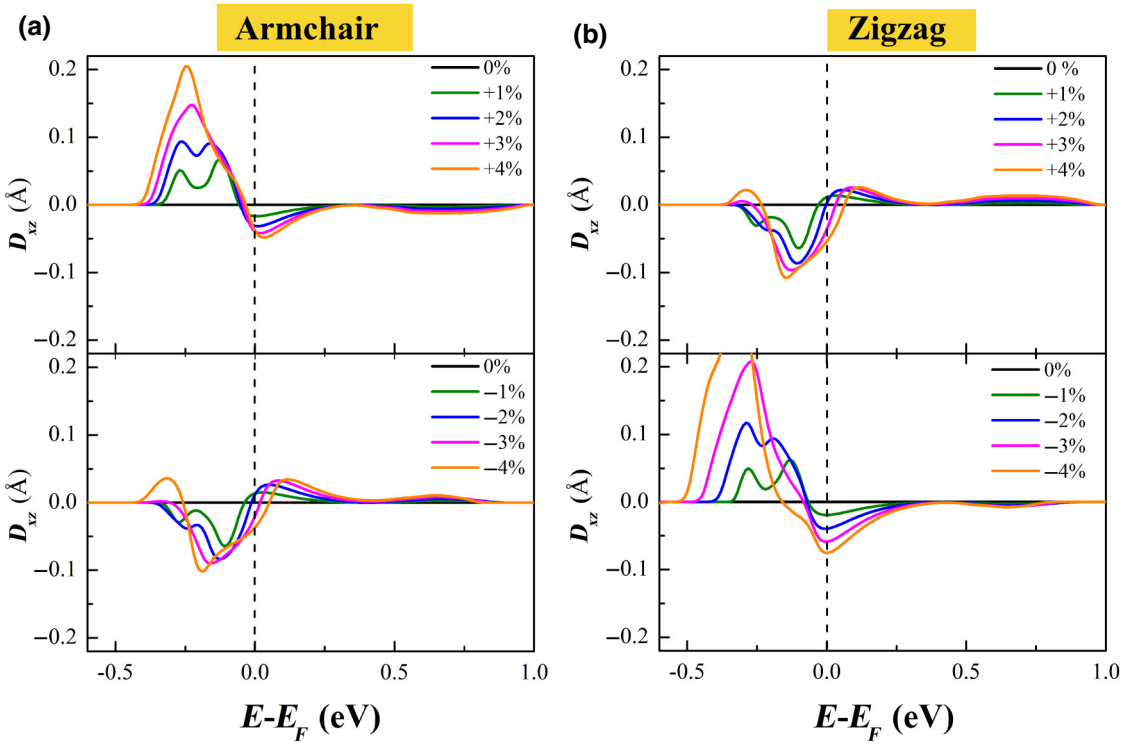

FIG. 4. D_{xz} of monolayer $1H$-NbS_2 under (a) armchair (b) zigzag strain, for which the positive (negative) strain value represents the tensile (compressive) strain.

Next, we estimate the nonlinear Hall signals that **D** induced. In 2D materials, the nonlinear Hall current density $J^{(2\omega)}$ is expressed as [41] [nonlinear Hall current density $J^{(0)}$ has a similar form with $J^{(2\omega)}$]

$$\begin{pmatrix} J_x^{(2\omega)} \\ J_y^{(2\omega)} \end{pmatrix} = \begin{pmatrix} 0 & \chi_{xxy} & 0 & \chi_{xyy} \\ \chi_{yxx} & 0 & \chi_{yyx} & 0 \end{pmatrix} \begin{pmatrix} E_x^2 \\ E_x E_y \\ E_y E_x \\ E_y^2 \end{pmatrix}, \tag{13}$$

where $E = \varepsilon e^{i\omega t}$ is the in-plane driving electric field, χ_{abc} is the nonlinear Hall coefficient

$$\begin{cases} \chi_{xyy} = e^3\tau/\left[2\hbar^2(1+i\omega\tau)\right]D_{yz}, \\ \chi_{yyx} = -e^3\tau/\left[2\hbar^2(1+i\omega\tau)\right]D_{yz}, \\ \chi_{xxy} = e^3\tau/\left[2\hbar^2(1+i\omega\tau)\right]D_{xz}, \\ \chi_{yxx} = -e^3\tau/\left[2\hbar^2(1+i\omega\tau)\right]D_{xz}, \end{cases} \tag{14}$$

here $-e$ is the electron charge, and τ is the relaxation time. In uniaxially strained $1H$-MX_2 (M = Nb, Ta; X = S, Se), only χ_{xxy} and χ_{yxx} are nonvanishing because of the nonzero D_{xz}. The second-order nonlinear Hall current density and the corresponding nonlinear Hall voltage perpendicular to the driving electric current are

$$\begin{cases} J_\perp^{(2\omega)} = \dfrac{\mathbf{J}^{(2\omega)} \times \mathbf{J}^{(\omega)}}{\left|\mathbf{J}^{(\omega)}\right|} = \dfrac{e^3\tau}{2\hbar^2(1+i\omega\tau)}|E|^2 D_{xz}\cos\theta, \\ V_\perp^{(2\omega)} = \dfrac{e^3\tau}{2\hbar^2(1+i\omega\tau)}\rho|E|^2 D_{xz} l\cos\theta, \end{cases} \tag{15}$$

where θ means the angle between the driving electric current and zigzag direction (i.e., direction of **D**), ρ means the resistivity, and l refers to the transverse length of the sample. The nonlinear Hall current is proportional to $|E|^2 D_{xz}\cos\theta$ [Eq. (15)]. It means that the nonlinear Hall voltage is maximum when the incident current is along the zigzag direction and vanishes when the incident current is along the armchair direction. The relationships among the strain, Berry-curvature dipole, and nonlinear Hall current are summarized in Fig. 5.

Taking typical driving current density $J^{(\omega)} \sim 10$ A/m [21], resistivity $\rho \sim 10^4$ Ω normalized from the bulk resistivity in $1H$-MX_2 (M = Nb, Ta; X = S, Se) [42], relaxation time $\tau \sim 10^{-14}$ s, and transverse length of the sample $l = 10$ μm, strain-induced $D_{xz} \sim 0.05$ Å (e.g., see Fig. 4) can generate Hall voltage of 10 μV, which is comparable to those measured in 2D WTe_2 [21,22]. Since strain can

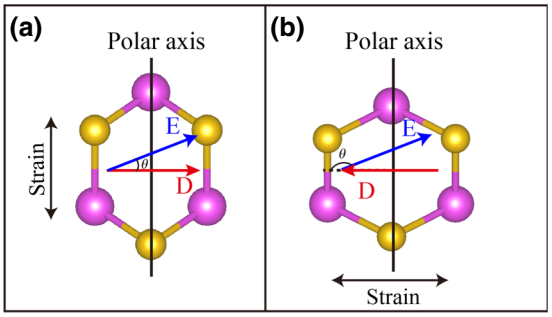

FIG. 5. Relationships between the strain, Berry-curvature dipole **D**, and nonlinear Hall current. **D** is always perpendicular to the polar axis under (a) armchair and (b) zigzag strain, while inverse to its direction in two kinds of strain. The nonlinear Hall current is proportional to $|E|^2 D_{xz} \cos\theta$, so the nonlinear Hall effect is maximum when the charge current is parallel to **D**.

switch the nonlinear Hall voltage from zero to an observable value, $1H$-MX_2 (M = Nb, Ta; X = S, Se) can be used in piezoelectriclike devices.

It needs to apply alternating current (ac) on the $1H$-MX_2 (M = Nb, Ta; X = S, Se) and control the strain as shown in Fig. 1 in real experiments. Our proposal is inspired by traditional 2D piezoelectricity devices such as MoS_2, which is an import 2D piezoelectricity device [13,14]. $1H$-MX_2 (M = Nb, Ta; X = S, Se) have similar crystal structures with 2D MoS_2, therefore our proposal is assessable in experiments based on the same setup with MoS_2. Freestanding bilayer 2D WTe_2 has a single mirror symmetry $\mathcal{M}_{yz}$, and can induce the nonzero Berry-curvature dipole D_{xz} [21–23,26,43]. Compared to D_{xz} in $1H$-MX_2 (M = Nb, Ta; X = S, Se) induced by uniaxial strain, D_{xz} is larger in bilayer WTe_2. However, there is no phase transition in bilayer WTe_2 when strain is applied, and its D_{xz} has no on-off effect. In the view of piezoelectriclike applications, $1H$-MX_2 (M = Nb, Ta; X = S, Se) are more suitable than bilayer 2D WTe_2.

V. CHARACTERISTICS OF PIEZOELECTRICLIKE DEVICES

Strain can break the symmetries and switch **P** and **D** in semiconductors and metals respectively, so these two kinds of piezoelectric effects are both sensitive to strain. The induced voltages all have positive correlations with strains. Except for the similarities of **P** and **D** discussed above, the method to fabricate the piezoelectriclike devices utilizing **D** is quite different from the traditional one based on **P** [12–18]. Traditional piezoelectric materials are semiconductors. The piezoelectricity is due to the variety of electric dipole **P** under strain, and thus the strain-induced electrons cannot move and accumulate on the surface of semiconductors. While the piezoelectriclike materials discussed here are metals, and strain-induced electrons can flow in them. Therefore, the response voltage in the 2D piezoelectriclike materials is less than that in traditional 2D piezoelectric semiconductors. Besides, the nonlinear Hall effect requires a finite bias to drive it. Therefore, the energy conversion efficiency of piezoelectriclike devices is low. Unlike traditional piezoelectric materials, they cannot be used as energy converters.

External voltage can introduce the strain in traditional piezoelectric materials, i.e., the inverse piezoelectric effect due to Onsager's reciprocal relations. The induced atom displacement constrains the application of the traditional piezoelectric materials in the fast ac region. Different from traditional piezoelectric materials, the 2D metallic materials lack Onsager's reciprocal relations, so external voltage almost cannot move atoms. The nonlinear effect is due to the response of free electrons, so the reaction time is much faster. Similar to nonlinear optics, nonlinear Hall effect causes the double frequency (ac) and zero frequency (dc) signal [see the description of Eq. (13)]. Because of the different output frequencies, it is very easy to separate the response signals from the driving ones, and the interference of the noise is small. These merits make it sensitive in signal detection and quick response. Moreover, the piezoelectriclike effect originates from Berry-curvature dipole, which is highly related to the topological properties of the Fermi surface, and thus the piezoelectriclike signal is robust against disorder. These are advantages in the piezoelectriclike applications induced by **D**. Therefore, 2D metallic piezoelectriclike materials can be used as strain sensors, terahertz detections, energy harvesters, etc. [22,44].

VI. CONCLUSION

In summary, uniaxial strain (along zigzag or armchair direction) can manipulate Berry-curvature dipole **D** in 2D metals $1H$-MX_2 (M = Nb, Ta; X = S, Se). Without strain, the $\mathcal{C}_{3z}$ symmetry eliminates the **D**. Uniaxial strain breaks the $\mathcal{C}_{3z}$ symmetry, and guarantees the existence of the nonzero **D**. The direction of **D** is perpendicular to the polar axis, different from the relationship between electric dipole **P** and polar axis. Uniaxial strain-induced Berry-curvature dipole **D** can generate observable nonlinear Hall signals under the experimental condition. The maximum nonlinear Hall effect can be obtained when the charge current is parallel to **D**. The nonlinear Hall signals have different frequencies with the driving current, which has advantages in the piezoelectriclike applications due to the convenience of detecting. $1H$-MX_2 (M = Nb, Ta; X = S, Se) can be used in piezoelectriclike devices based on Berry-curvature dipole **D**. The piezoelectriclike property utilizing **D** in metals is quite different from the traditional one in insulators based on **P**, due to the nonlinear and topological properties of **D**. The piezoelectriclike devices can be used as strain probe or sensor, high-frequency rectifier, low-power

energy harvester, terahertz detection, wireless charger, etc. We hope our prediction can expand the potential piezoelectriclike application in 2D metallic materials.

ACKNOWLEDGMENTS

This work is supported by the NBRP of China (2019YFA0308403), the National Nature Science Foundation of China under Grants No. 11822407 and No. 11947212, the China Postdoctoral Science Foundation No. 2018M640513, and a Project Funded by the Priority Academic Program Development of Jiangsu Higher Education Institutions.

APPENDIX A: d_{xz} AND d_{yz} UNDER $\mathcal{C}_{3z}$ SYMMETRY

The $\mathcal{C}_{3z}$ rotation symmetry transforms the point A in the Fermi surface to points B and C, as shown in Fig. 6. $\Omega_z(A) = \Omega_z(B) = \Omega_z(C)$ and $\mathbf{v}(A) + \mathbf{v}(B) + \mathbf{v}(C) = 0$ due to the $\mathcal{C}_{3z}$ symmetry. Therefore, the integration of the d_{xz} and d_{yz} over the Brillouin zone leads to the vanishing of D_{xz} and D_{yz} due to $[v_x(A)\Omega_z(A) + v_x(B)\Omega_z(B) + v_x(C)\Omega_z(C)]\Omega_z = 0$ and $[v_y(A)\Omega_z(A) + v_y(B)\Omega_z(B) + v_y(C)\Omega_z(C)]\Omega_z = 0$.

APPENDIX B: D_{xz} OF 1H-$NbSe_2$, 1H-TaS_2 AND 1H-$TaSe_2$ UNDER ARMCHAIR STRAIN

The Berry-curvature dipole under armchair strain for 1H-$NbSe_2$, 1H-TaS_2, and 1H-$TaSe_2$ are plotted in Fig. 7.D_{xz} changes linearly with strain, and the strain effects on D_{xz} of 1H-$NbSe_2$ and the 1H-$TaSe_2$ are more significant than that of 1H-NbS_2 and 1H-TaS_2. The Berry curvature relates to the competition between the spin-orbit coupling effect and bandgap. The 1H-$NbSe_2$ can reach a more significant strain effect due to the smaller gap between lower valence bands, even though the spin-orbit coupling is not the strongest.

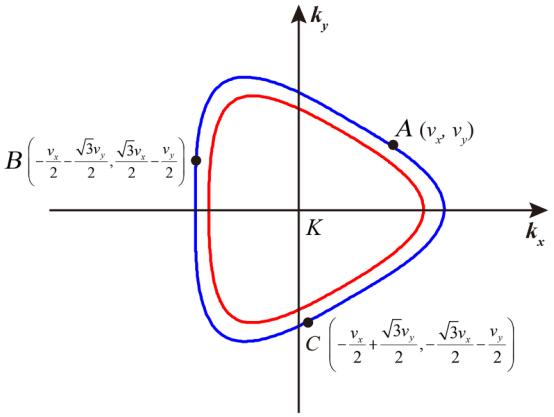

FIG. 6. Velocity relationships between the symmetry points around the K point under the $\mathcal{C}_{3z}$ symmetry.

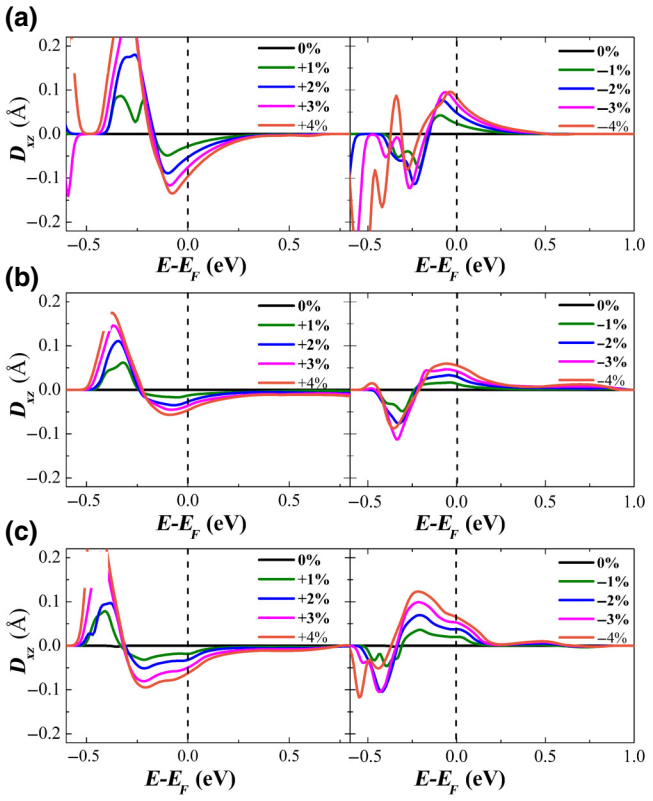

FIG. 7. D_{xz} of (a) 1H-$NbSe_2$, (b) 1H-TaS_2, and (c) 1H-$TaSe_2$ under different armchair strains.

[1] Z. L. Wang and W. Wu, Piezotronics and piezophototronics: Fundamentals and applications, Natl. Sci. Rev. **1**, 62 (2013).
[2] P. Fei, P. H. Yeh, J. Zhou, S. Xu, Y. Gao, J. Song, Y. Gu, Y. Huang, and Z. L. Wang, Piezoelectric potential gated field-effect transistor based on a free-standing ZnO wire, Nano Lett. **9**, 3435 (2009).
[3] J. He, C. Hsin, J. Liu, L. Chen, and Z. Wang, Piezoelectric gated diode of a single ZnO nanowire, Adv. Mater. **19**, 781 (2007).
[4] A. I. Kingon and S. Srinivasan, Lead zirconate titanate thin films directly on copper electrodes for ferroelectric, dielectric and piezoelectric applications, Nat. Mater. **4**, 233 (2005).
[5] W. Liu, M. Lee, L. Ding, J. Liu, and Z. L. Wang, Piezopotential gated nanowire-nanotube hybrid field-effect transistor, Nano Lett. **10**, 3084 (2010).
[6] X. Wang, J. Zhou, J. Song, J. Liu, N. Xu, and Z. L. Wang, Piezoelectric field effect transistor and nanoforce sensor based on a single ZnO nanowire, Nano Lett. **6**, 2768 (2006).
[7] Z. Wang, Nanopiezotronics, Adv. Mater. **19**, 889 (2007).
[8] Z. L. Wang and J. Song, Piezoelectric nanogenerators based on zinc oxide nanowire arrays, Science **312**, 242 (2006).
[9] W. Wu, Y. Wei, and Z. L. Wang, Strain-gated piezotronic logic nanodevices, Adv. Mater. **22**, 4711 (2010).

[10] R. Yang, Y. Qin, L. Dai, and Z. L. Wang, Power generation with laterally packaged piezoelectric fine wires, Nat. Nanotechnol. **4**, 34 (2008).

[11] J. Zhou, Y. Gu, P. Fei, W. Mai, Y. Gao, R. Yang, G. Bao, and Z. L. Wang, Flexible piezotronic strain sensor, Nano Lett. **8**, 3035 (2008).

[12] K.-A. N. Duerloo, M. T. Ong, and E. J. Reed, Intrinsic piezoelectricity in two-dimensional materials, J. Phys. Chem. Lett. **3**, 2871 (2012).

[13] W. Wu, L. Wang, Y. Li, F. Zhang, L. Lin, S. Niu, D. Chenet, X. Zhang, Y. Hao, T. F. Heinz, J. Hone, and Z. L. Wang, Piezoelectricity of single-atomic-layer MoS_2 for energy conversion and piezotronics, Nature **514**, 470 (2014).

[14] H. Zhu, Y. Wang, J. Xiao, M. Liu, S. Xiong, Z. J. Wong, Z. Ye, Y. Ye, X. Yin, and X. Zhang, Observation of piezoelectricity in free-standing monolayer MoS_2, Nat. Nanotechnol. **10**, 151 (2014).

[15] M. Birkholz, Crystal-field induced dipoles in heteropolar crystals II: Physical significance, Zeitschrift für Physik B Condensed Matter **96**, 333 (1995).

[16] S. Bertolazzi, J. Brivio, and A. Kis, Stretching and breaking of ultrathin MoS_2, ACS Nano **5**, 9703 (2011).

[17] C. Lee, X. Wei, J. W. Kysar, and J. Hone, Measurement of the elastic properties and intrinsic strength of monolayer graphene, Science **321**, 385 (2008).

[18] M. N. Blonsky, H. L. Zhuang, A. K. Singh, and R. G. Hennig, Ab initio prediction of piezoelectricity in two-dimensional materials, ACS Nano **9**, 9885 (2015).

[19] I. Sodemann and L. Fu, Quantum Nonlinear Hall Effect Induced by Berry Curvature Dipole in Time-Reversal Invariant Materials, Phys. Rev. Lett. **115**, 216806 (2015).

[20] T. Low, Y. Jiang, and F. Guinea, Topological currents in black phosphorus with broken inversion symmetry, Phys. Rev. B **92**, 235447 (2015).

[21] K. Kang, T. Li, E. Sohn, J. Shan, and K. F. Mak, Observation of the nonlinear anomalous Hall effect in 2D WTe_2, Nat. Mater. **18**, 324 (2019).

[22] Q. Ma *et al.*, Observation of the nonlinear Hall effect under time-reversal-symmetric conditions, Nature **565**, 337 (2019).

[23] S.-Y. Xu, Q. Ma, H. Shen, V. Fatemi, S. Wu, T.-R. Chang, G. Chang, A. M. M. Valdivia, C.-K. Chan, Q. D. Gibson, J. Zhou, Z. Liu, K. Watanabe, T. Taniguchi, H. Lin, R. J. Cava, L. Fu, N. Gedik, and P. Jarillo-Herrero, Electrically switchable Berry curvature dipole in the monolayer topological insulator WTe_2, Nat. Phys. **14**, 900 (2018).

[24] M. Ashton, J. Paul, S. B. Sinnott, and R. G. Hennig, Topology-Scaling Identification of Layered Solids and Stable Exfoliated 2D Materials, Phys. Rev. Lett. **118**, 106101 (2017).

[25] N. Mounet, M. Gibertini, P. Schwaller, D. Campi, A. Merkys, A. Marrazzo, T. Sohier, I. E. Castelli, A. Cepellotti, G. Pizzi, and N. Marzari, Two-dimensional materials from high-throughput computational exfoliation of experimentally known compounds, Nat. Nanotechnol. **13**, 246 (2018).

[26] J.-S. You, S. Fang, S.-Y. Xu, E. Kaxiras, and T. Low, Berry curvature dipole current in the transition metal dichalcogenides family, Phys. Rev. B **98**, 121109 (2018).

[27] B. T. Zhou, C.-P. Zhang, and K. T. Law, arXiv:1903.11958 (2019).

[28] J. Kim, K. W. Kim, D. Shin, S. H. Lee, J. Sinova, N. Park, and H. Jin, Prediction of ferroelectricity-driven Berry curvature enabling charge- and spin-controllable photocurrent in tin telluride monolayers, Nat. Commun. **10**, 3965 (2019).

[29] H. Wang and X. Qian, Ferroicity-driven nonlinear photocurrent switching in time-reversal invariant ferroic materials, Sci. Adv. **5**, eaav9743 (2019).

[30] P. Giannozzi *et al.*, Quantum Espresso: A modular and open-source software project for quantum simulations of materials, J. Phys.: Condens. Matter **21**, 395502 (2009).

[31] A. A. Mostofi, J. R. Yates, Y.-S. Lee, I. Souza, D. Vanderbilt, and N. Marzari, Wannier90: A tool for obtaining maximally-localised Wannier functions, Comput. Phys. Commun. **178**, 685 (2008).

[32] A. A. Mostofi, J. R. Yates, G. Pizzi, Y.-S. Lee, I. Souza, D. Vanderbilt, and N. Marzari, An updated version of Wannier90: A tool for obtaining maximally-localised Wannier functions, Comput. Phys. Commun. **185**, 2309 (2014).

[33] Q. Wu, S. Zhang, H.-F. Song, M. Troyer, and A. A. Soluyanov, Wanniertools: An open-source software package for novel topological materials, Comput. Phys. Commun. **224**, 405 (2018).

[34] H. Ryu, Y. Chen, H. Kim, H. Z. Tsai, S. Tang, J. Jiang, F. Liou, S. Kahn, C. Jia, A. A. Omrani, J. H. Shim, Z. Hussain, Z. X. Shen, K. Kim, B. I. Min, C. Hwang, M. F. Crommie, and S. K. Mo, Persistent charge-density-wave order in single-layer $TaSe_2$, Nano Lett. **18**, 689 (2018).

[35] N. E. Staley, J. Wu, P. Eklund, Y. Liu, L. Li, and Z. Xu, Electric field effect on superconductivity in atomically thin flakes of $NbSe_2$, Phys. Rev. B **80**, 184505 (2009).

[36] M. M. Ugeda, A. J. Bradley, Y. Zhang, S. Onishi, Y. Chen, W. Ruan, C. Ojeda-Aristizabal, H. Ryu, M. T. Edmonds, H.-Z. Tsai, A. Riss, S.-K. Mo, D. Lee, A. Zettl, Z. Hussain, Z.-X. Shen, and M. F. Crommie, Characterization of collective ground states in single-layer $NbSe_2$, Nat. Phys. **12**, 92 (2016).

[37] X. Xi, H. Berger, L. Forró, J. Shan, and K. F. Mak, Gate Tuning of Electronic Phase Transitions in Two-Dimensional $NbSe_2$, Phys. Rev. Lett. **117**, 106801 (2016).

[38] X. Xi, Z. Wang, W. Zhao, J.-H. Park, K. T. Law, H. Berger, L. Forro, J. Shan, and K. F. Mak, Ising pairing in superconducting $NbSe_2$ atomic layers, Nat. Phys. **12**, 139 (2016).

[39] X. Xi, L. Zhao, Z. Wang, H. Berger, L. Forró, J. Shan, and K. F. Mak, Strongly enhanced charge-density-wave order in monolayer $NbSe_2$, Nat. Nanotechnol. **10**, 765 (2015).

[40] J. Son, K.-H. Kim, Y. H. Ahn, H.-W. Lee, and J. Lee, Strain Engineering of the Berry Curvature Dipole and Valley Magnetization in Monolayer MoS_2, Phys. Rev. Lett. **123**, 036806 (2019).

[41] Z. Z. Du, C. M. Wang, H. Z. Lu, and X. C. Xie, Band Signatures for Strong Nonlinear Hall Effect in Bilayer WTe_2, Phys. Rev. Lett. **121**, 266601 (2018).

[42] M. Naito and S. Tanaka, Electrical transport properties in 2*H*-NbS_2, -$NbSe_2$, -TaS_2 and -$TaSe_2$, J. Phys. Soc. Jpn. **51**, 219 (1982).

[43] Y. Zhang, J. van den Brink, C. Felser, and B. Yan, Electrically tuneable nonlinear anomalous Hall effect in two-dimensional transition-metal dichalcogenides WTe_2 and $MoTe_2$, 2D Mater. **5**, 044001 (2018).

[44] H. Isobe, S.-Y. Xu, and L. Fu, arXiv:1812.08162 (2018).